INTERNATIONAL JOURNAL FOR NUMERICAL METHODS IN FLUIDS, VOL. 11, 953–967 (1990)

A TEST PROBLEM FOR OUTFLOW BOUNDARY CONDITIONS—FLOW OVER A BACKWARD-FACING STEP

DAVID K. GARTLING

Fluid and Thermal Sciences Department, Sandia National Laboratories, Albuquerque, NM 87185, U.S.A.

SUMMARY

A numerical solution for steady incompressible flow over a two-dimensional backward-facing step is developed using a Galerkin-based finite element method. The Reynolds number for the simulations is 800. Computations are performed on an extended channel length to minimize the effect of the outflow boundary on the upstream recirculation zones. A thorough mesh refinement study is performed to validate the results. Extensive profile data at several channel locations are provided to allow future testing and evaluation of outflow boundary conditions.

KEY WORDS Finite element Navier–Stokes Outflow boundary conditions Backward-facing step

1. INTRODUCTION

The selection of an outflow boundary condition that allows an accurate numerical simulation of a flow problem to be achieved continues to be an area of uncertainty and debate. The Navier–Stokes equations provide a widely applicable mathematical description for the analysis of fluid motion. Individual flow problems are differentiated by specific choices of fluid properties, the geometry of interest and a suitable set of boundary and initial conditions for the flow variables. Generally, the boundary conditions are the most difficult to define (precisely) since it is difficult to isolate a fluid system from the effects of its environment. This is particularly true for uncontained flows, which require some rational specification of how the fluid enters and leaves the domain of interest.

The primary function of any outflow boundary condition used in a numerical simulation is to allow the flow variables to leave the computational grid passively without perturbing the upstream flow. Optimally, such a boundary condition would be applicable at any downstream location so that the extent of the computational domain could be minimized. The interest in developing better outflow boundary conditions remains high as seen by the success of the Minisymposium on Outflow Boundary Conditions held at the University College of Swansea, U.K. in July 1989. As part of that forum a series of standard problems were defined that could be used to test (quantitatively) various outflow specifications. In each case the standard problem was to be solved on a computational mesh of sufficient refinement and streamwise extent that it could be deemed a 'true' solution to the boundary value problem. The present paper is a report on one of those standard problems consisting of steady incompressible flow over a backward-facing step. It is the intention of this work to provide relevant data in a format that can be used for future testing and evaluation of outflow boundary conditions.

0271–2091/90/150953–15$07.50

Received 12 February 1990
Revised 9 May 1990

The paper is organized as follows. Section 2 describes the problem geometry and flow parameters of interest. Sections 3 and 4 outline the numerical method and computational models used for the simulations. Section 4 provides a variety of results, in both tabular and graphical form, that define the flow and demonstrate that the numerical results are converged and valid.

2. BACKWARD-FACING STEP

The problem involving a steady viscous incompressible flow over an isothermal two-dimensional backward-facing step is a standard test problem that has been addressed by numerous authors using a wide variety of numerical methods. Since the problem defined here is intended to provide a basis for the comparison of various outflow boundary conditions, the standard step geometry was simplified by excluding the channel upstream of the step. As shown in Figure 1, the downstream channel was defined to have unit height H with a step height and upstream inlet region set equally to $H/2$. For purposes of generating the baseline solution to this problem, the downstream channel length was taken as $L=30\ H$, i.e. the channel extends 60 step heights from the inlet. The co-ordinate system for describing locations in the channel is centred at the step corner with the x-co-ordinate being defined as positive in the downstream direction and the y-co-ordinate across the channel.

The boundary conditions for the step geometry included the usual no-slip velocity specification for all solid surfaces (see Figure 1). The inlet velocity field was specified as a parallel flow with a parabolic horizontal component given by $u(y)=24y(0{\cdot}5-y)$ for $0\leqslant y\leqslant 0{\cdot}5$. This produces a maximum inflow velocity of $u_{max}=1{\cdot}5$ and an average inflow velocity of $u_{avg}=1{\cdot}0$. The outflow boundary condition assumed a parallel flow and a constant total stress normal to the boundary. The normal stress condition translates into $-P+2\mu\,\partial u/\partial x$ being specified as a constant, where P is the pressure, μ the fluid viscosity and u the axial velocity component. For these computations the constant was set to zero, which in essence sets the outflow pressure to zero since the term $\mu\,\partial u/\partial x$ is negligible at this streamwise station. After a solution had been obtained, the pressure field was adjusted such that the pressure level was zero at the step corner ($x=0$, $y=0$).

For convenience in setting the required flow conditions, the non-dimensional form of the Navier–Stokes equations was employed. For a fixed geometry this results in the Reynolds number being the only non-dimensional parameter of interest; the Reynolds number is defined by $Re=u_{avg}H/\nu$. To provide the required baseline solution at $Re=800$, the kinematic viscosity ν was adjusted in concert with the specified u_{avg} and H. The Reynolds number and problem definition used here follow Armaly *et al.*,[1] which will allow the comparison of some computed results in a subsequent section.

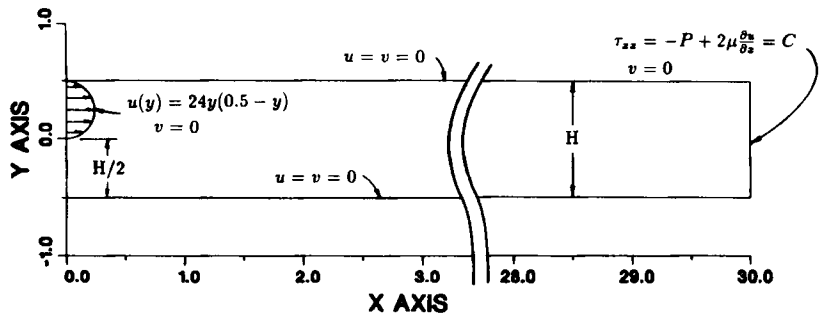

Figure 1. Backward-facing step geometry with channel dimensions and boundary conditions

3. NUMERICAL METHOD

The numerical solution to the step flow was carried out using the code NACHOS II,[2] which is based on a Galerkin finite element formulation. Verification of selected results was performed using the FIDAP program,[3] which is also based on the finite element method. In all cases the primitive variable form of the Navier–Stokes equations was employed with a mixed finite element approximation used to represent the velocity components and pressure in the momentum equations and incompressibility constraint. The quadrilateral finite element used for all reported computations contained a nine-node biquadratic Lagrange interpolation for the velocity components; the pressure approximation was linear and discontinuous between elements. For comparison purposes, results were also obtained using the nine-node velocity, four-node continuous bilinear pressure element. No significant differences were seen between the solutions using the two element types, though the element mass balance for the linear pressure element was superior as anticipated.

The backward step flow was formulated and solved as a steady flow problem. In order to obtain a solution for the specified *Re* of 800, a series of steady state solutions were obtained at intermediate *Re*-values of 200, 400 and 600. Zeroth-order continuation was used to advance from one *Re* solution to another. The indicated sequence of steps in *Re* does not represent an optimized path to the final required state but was selected for convenience and with a view towards comparing solutions at other standard conditions. The continuation procedure was employed for all solutions except those obtained on the most refined computational mesh. In order to expedite these large mesh computations, solution fields from converged, coarser mesh solutions were interpolated to the refined mesh[4] to provide a good initial estimate of the solution.

At each *Re*, full Newton iteration was used to obtain a converged solution for the non-linear algebraic equations. A convergence tolerance of 0·1% on the normalized change in the solution vectors between iterations was used to terminate the iteration scheme; typically, less than eight iterations were needed at each *Re* to obtain converged solutions. A direct solver employing the frontal technique for Gauss elimination[2] was used to solve the unsymmetric matrix problem at each Newton iteration.

In addition to the primary velocity and pressure variables, a number of derived variables were computed as part of the benchmark. The streamfunction was computed from a line integral of the velocity components taken between nodal points along element edges. This procedure also provided a check on the divergence of the velocity field within each element; the maximum error in the streamfunction (velocity divergence) around any element was $\sim 10^{-9}$. To maximize the accuracy in the variables obtained through differentiation (e.g. velocity gradients, stress components and vorticity), all velocity derivatives were evaluated at the 2×2 Gauss points within each element. Gauss point values were subsequently projected to the corner nodes of the element via a bilinear extrapolation and averaged between adjacent elements to obtain a continuous field. For plotting purposes, midside node data were linearly interpolated from corner node data.

4. COMPUTATIONAL MODELS

In an effort to demonstrate that the reported solutions are converged in the mesh refinement sense, computations were performed on five meshes of (almost) uniformly increasing refinement. For convenience the meshes are labelled A–E and had finite element discretizations ranging from 720 to 32 000 elements. Specific details of each mesh are given in Table I.

The rectangular channel downstream of the step was divided into two regions for purposes of mesh generation. In the upstream region $0 \leqslant x \leqslant 15$ the mesh was uniformly distributed across the

Table I. Mesh characteristics

Mesh	Number of elements	Number of nodes*	Number of unknowns†	Element size‡ (Δx, Δy)	Matrix front width	Matrix solution time§ (s)
A	720 (6 × 120)	3133	8426	0·166	61	12·4
B	2000 (10 × 200)	8421	22842	0·100	77	63·8
C	8000 (20 × 400)	32841	89682	0·050	117	720·0
D	18000 (30 × 600)	73261	200522	0·033	157	3050·1
E	32000 (40 × 800)	129681	355362	0·025	197	9515·5

* Nine nodes per element.
† Biquadiatic velocity, linear discontinuous pressure element.
‡ Length of element side for uniform grid region.
§ Time per iteration, includes matrix assembly, triangularization and backsubstitution.

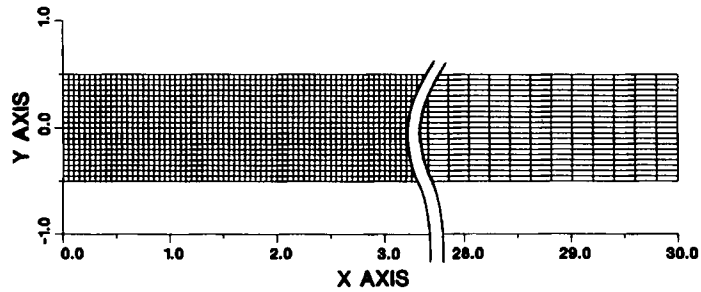

Figure 2. Finite element mesh distribution, mesh C

channel and in the streamwise direction. For the region $15 \leqslant x \leqslant 30$ the mesh was uniform across the channel but smoothly graded in the flow direction. The grading factor was two, so that elements near $x = 30$ were approximately twice the length of elements near $x = 15$. For each mesh three-quarters of the total number of elements were located in the upstream region. A schematic of mesh C is shown in Figure 2.

As shown in Table I, meshes B–E represent uniform refinements in both the cross-channel and downstream directions. Mesh A is not a uniform coarsening of mesh B owing to the need to retain an integer number of elements across the inflow section of the upstream boundary for the purpose of accurate boundary condition specification. However, these mesh configurations do correspond to almost an order-of-magnitude change in mesh size, which is sufficient to demonstrate convergence.

Included in Table I are some measures of problem size and performance of the finite element code. Note that all problems were run on a single processor of a CRAY X-MP/416 using a FORTRAN 77 compiler and the Cray Time Sharing System (CTSS). The code makes extensive use of the 256 Mword solid state disc (SSD) that is attached to the mainframe. The programme

also employs a dynamic memory manager that increases and decreases memory allocation on request. As a result, all five of the indicated meshes used different amounts of central memory and had different I/O patterns.

5. RESULTS

The results of the computations for the backward-facing step will be described in two subsections. In the first subsection, specific solution quantities such as vortex location and strength, separation length, etc. will be discussed as a function of mesh refinement. Having established that solutions on a particular mesh are converged and accurate, a standard set of cross-channel and streamwise profiles will be discussed for a variety of dependent variables. These quantities will be supplied at stations that are suitable for evaluating various outflow boundary conditions.

5.1. Mesh refinement results

The basic character of the backward-facing step flow at $Re = 800$ is well known and is illustrated in the contour plots of Figures 3–6. Note that these plots are to full scale but only show the first 20 step heights of the channel since few phenomena of interest occur downstream of this point. The flow separates at the step corner and forms a large recirculation eddy with a reattachment point on the lower wall approximately 12 step heights downstream. A second, stronger eddy forms on the upper wall beginning approximately 10 step heights downstream and terminating at 21 step heights. The streamfunction contours in Figure 3 illustrate the main features of the separated flow while the pressure contours in Figure 4 show clearly the pressure gradients associated with the various points of separation and reattachment. Note that the vorticity shown in Figure 5 is defined in the standard way as the curl of the velocity (i.e. $\omega = \partial v/\partial x - \partial u/\partial y$); the fluid speed in Figure 6 is simply the magnitude of the velocity. After reattachment of the upper wall eddy, the flow slowly recovers towards a fully developed Poiseuille flow. The return to a fully developed flow is almost complete in the channel length of 60 step heights used in these computations. Figures 7 and 8 show the pressure and shear stress distributions on the upper and lower walls. Note that near the exit plane the pressure closely approaches a constant slope consistent with a fully developed flow and the shear stress reaches a nearly constant value. The maximum outflow velocity is within 1% of a fully developed parabolic

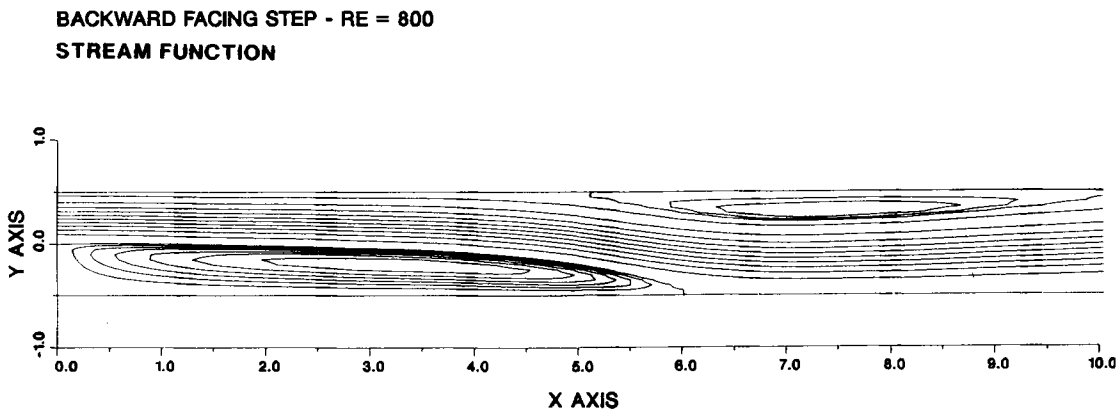

Figure 3. Streamfunction contours. Level values are −0·030, −0·025, −0·020, −0·015, −0·010, −0·005, 0·0, 0·050, 0·100, 0·150, 0·200, 0·250, 0·300, 0·350, 0·400, 0·450, 0·490, 0·500, 0·502, 0·504

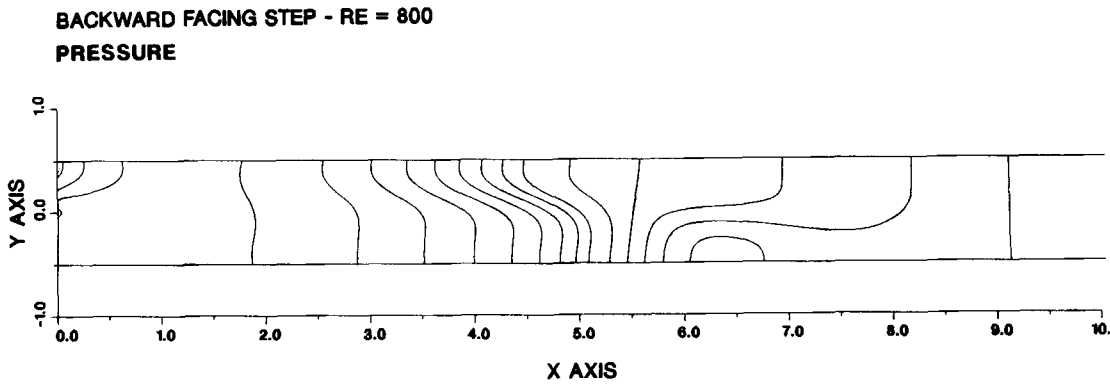

Figure 4. Pressure contours. Level values are 0·01, 0·02, 0·03, 0·04, 0·05, 0·06, 0·07, 0·08, 0·09, 0·10, 0·12, 0·14, 0·16, 0·18, 0·20, 0·22, 0·24

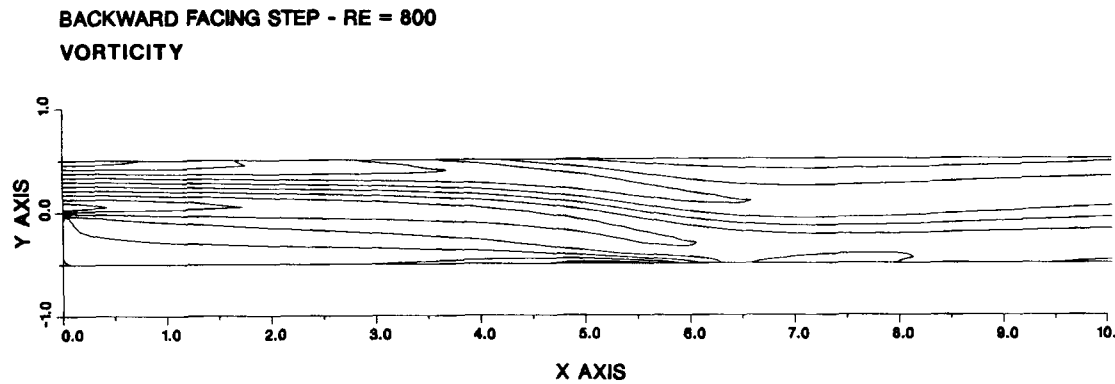

Figure 5. Vorticity contours. Level values are 10·0, 8·0, 6·0, 4·0, 2·0, 0·0, −2·0, −4·0, −6·0, −8·0

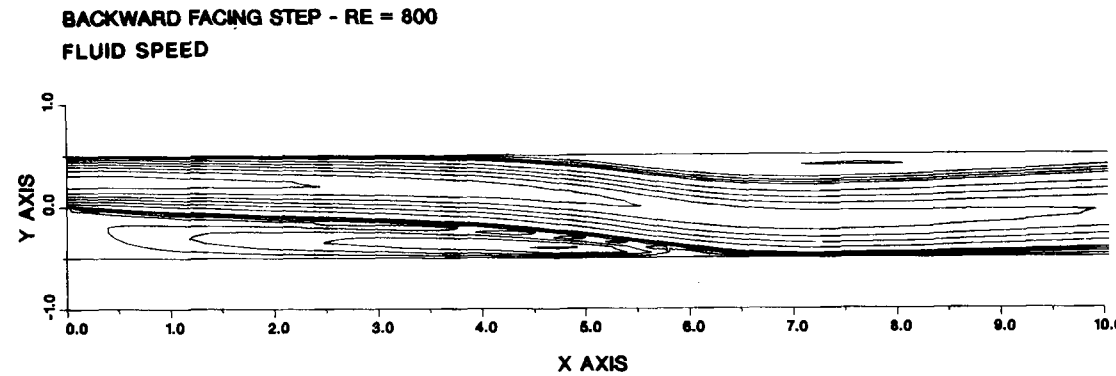

Figure 6. Contours of fluid speed. Level values are 0·05, 0·10, 0·15, 0·20, 0·40, 0·60, 0·80, 1·00, 1·20, 1·40

profile. This evidence supports the conclusion that the computational domain is of sufficient length to provide an accurate solution for regions close to the step.

Listed in Tables II and III are specific details regarding the two separation zones known to be present in the channel. These quantities are listed versus mesh configuration and clearly show the

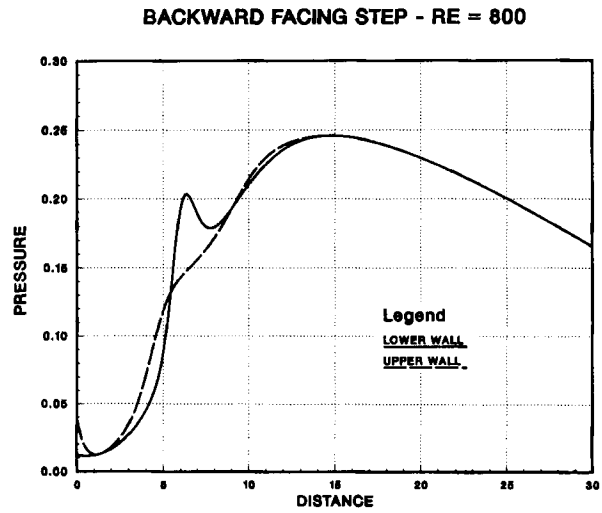

Figure 7. Pressure profiles along upper and lower channel walls

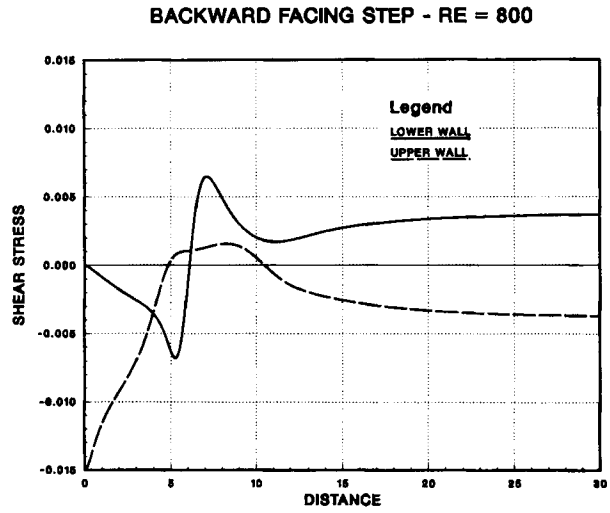

Figure 8. Shear stress profiles along upper and lower channel walls

rapid approach to mesh-independent values. The mesh B results are within 1·5% of the most refined mesh quantities, demonstrating that quite accurate solutions can be obtained on rather modest refinements. The vorticity at the centre of each vortex shows the most variation between meshes. This is to be expected for this formulation since it is a derivative quantity and of lower-order accuracy than the primary fields. Note that the quantities associated with the vortex centres were taken directly from values computed at the node points. The separation and reattachment points were located from the wall shear stress; interpolation between nodal point shear stress values was used to locate the zero-shear-stress point. The values listed in Tables II and III were all

Table II. Lower wall eddy

Mesh	Vortex centre (x, y)	Stream function at vortex centre, ψ	Vorticity at vortex centre, ω	Length of recirculation region, L_1
A	(3·000, −0·167)	−0·0335	−2·518	5·81
B	(3·300, −0·200)	−0·0342	−2·249	6·07
C	(3·350, −0·200)	−0·0342	−2·285	6·09
D	(3·350, −0·200)	−0·0342	−2·283	6·10
E	(3·350, −0·200)	−0·0342	−2·283	6·10

Table III. Upper wall eddy

Mesh	Vortex centre (x, y)	Streamfunction at vortex centre, ψ	Vorticity at vortex centre, ω	Separation point (x, y)	Reattachment point (x, y)	Length of recirculation region, L_u
A	(7·500, 0·333)	0·5071	0·959	(4·79, 0·50)	(10·48, 0·50)	5·69
B	(7·400, 0·300)	0·5064	1·319	(4·83, 0·50)	(10·47, 0·50)	5·64
C	(7·400, 0·300)	0·5064	1·321	(4·85, 0·50)	(10·48, 0·50)	5·63
D	(7·400, 0·300)	0·5064	1·324	(4·85, 0·50)	(10·48, 0·50)	5·63
E	(7·400, 0·300)	0·5064	1·322	(4·85, 0·50)	(10·48, 0·50)	5·63

obtained from the NACHOS II programme; comparison of mesh C and D results with quantities obtained from FIDAP agreed within the significant figures shown in the table.

The flow statistics listed in the tables can, with some caution, be compared with results from other experimental and numerical investigations. Armaly *et al.*[1] measured separation and reattachment points for a wide range of Reynolds numbers including the case of $Re = 800$. Unfortunately, three-dimensional effects in the channel appear to be significant for $Re > 400$, making comparisons with two-dimensional simulations less than satisfactory. Data from Reference 1 suggest that the lower wall separation zone has a dimensional length of $L_1 \approx 7{\cdot}2$; the upper wall separation region has a length $L_u \approx 4{\cdot}1$ with separation beginning at $x \approx 5{\cdot}3$. Comparison of these values with the results in Tables II and III clearly shows the discrepancies between experiment and numerical predictions. In comparing the present results with other two-dimensional computations, somewhat better agreement is realized, especially with respect to the lower wall separation zone. Kim and Moin[5] predicted separation lengths of $L_1 \approx 6{\cdot}0$ and $L_u \approx 5{\cdot}75$ using a finite difference method. Sohn[6] used the FIDAP code to predict $L_1 \approx 5{\cdot}8$ and $L_u \approx 4{\cdot}7$. Exceptionally accurate quantities are difficult to obtain from these investigations since no tabular results were given; graphical results were optically scanned and interpolated to produce the cited quantities. Note that in both of these cases relatively modest mesh refinements were used on channel geometries that extended only 30 step heights downstream of the step. In view of the good convergence behaviour shown in Tables II and III, the use of an extended channel length and the exceptional agreement between two different computer codes, the present results are judged to be an accurate representation of the two-dimensional step flow. Unfortunately, experimental verification of this claim cannot be obtained since a strictly two-dimensional flow at these conditions apparently does not exist.

Table IV. Cross-channel profiles, $x = 7$

y	u	v ($\times 10^{-2}$)	P	$\omega=(\partial v/\partial x-\partial u/\partial y)$	$\partial u/\partial x$ ($\times 10^{-1}$)	$\partial u/\partial y$	$\partial v/\partial x$ ($\times 10^{-1}$)	$-P+\mu\partial u/\partial x$	$-P+2\mu\partial u/\partial x$	$\partial u/\partial y+\partial y/\partial x$
0·50	0·000	0·000	0·1562	−1·034	−0·006	1·034	−0·000	−0·1562	−0·1562	1·034
0·45	−0·038	−0·027	0·1562	−0·493	−0·102	0·493	−0·000	−0·1562	−0·1563	0·493
0·40	−0·049	−0·086	0·1562	0·061	−0·132	−0·061	0·004	−0·1563	−0·1563	−0·060
0·35	−0·032	−0·147	0·1562	0·635	−0·112	−0·633	0·019	−0·1562	−0·1563	−0·631
0·30	0·015	−0·193	0·1562	1·237	−0·071	−1·232	0·049	−0·1562	−0·1562	−1·227
0·25	0·092	−0·225	0·1562	1·888	−0·053	−1·878	0·100	−0·1562	−0·1562	−1·868
0·20	0·204	−0·268	0·1563	2·588	−0·115	−2·570	0·179	−0·1564	−0·1564	−2·552
0·15	0·349	−0·362	0·1567	3·267	−0·262	−3·238	0·289	−0·1567	−0·1567	−3·209
0·10	0·522	−0·544	0·1574	3·751	−0·466	−3·708	0·426	−0·1575	−0·1576	−3·665
0·05	0·709	−0·823	0·1590	3·821	−0·646	−3·764	0·576	−0·1591	−0·1591	−3·706
0·00	0·885	−1·165	0·1615	3·345	−0·718	−3·274	0·715	−0·1616	−0·1617	−3·202
−0·05	1·024	−1·507	0·1652	2·362	−0·644	−2·280	0·821	−0·1653	−0·1654	−2·197
−0·10	1·105	−1·778	0·1697	1·046	−0·440	−0·958	0·875	−0·1698	−0·1698	−0·871
−0·15	1·118	−1·925	0·1746	−0·374	−0·149	0·462	0·872	−0·1746	−0·1746	0·548
−0·20	1·062	−1·917	0·1792	−1·684	0·178	1·766	0·812	−0·1792	−0·1792	1·847
−0·25	0·948	−1·748	0·1831	−2·719	0·492	2·790	0·706	−0·1830	−0·1830	2·861
−0·30	0·792	−1·423	0·1859	−3·392	0·762	3·448	0·568	−0·1858	−0·1857	3·505
−0·35	0·613	−1·000	0·1876	−3·658	0·982	3·699	0·412	−0·1875	−0·1874	3·740
−0·40	0·428	−0·504	0·1885	−3·687	0·991	3·712	0·242	−0·1884	−0·1883	3·736
−0·45	0·232	−0·118	0·1888	−4·132	0·523	4·139	0·072	−0·1888	−0·1887	4·146
−0·50	0·000	0·000	0·1889	−5·140	−0·024	5·139	−0·012	−0·1889	−0·1889	5·138

Table V. Cross-channel profiles, $x = 15$

y	u	v ($\times 10^{-2}$)	P	$\omega=(\partial v/\partial x-\partial u/\partial y)$	$\partial u/\partial x$ ($\times 10^{-1}$)	$\partial u/\partial y$	$\partial v/\partial x$ ($\times 10^{-3}$)	$-P+\mu\partial u/\partial x$	$-P+2\mu\partial u/\partial x$	$\partial u/\partial y+\partial y/\partial x$
0·50	0·000	0·000	0·2460	2·027	0·003	−2·027	0·007	−0·2459	−0·2459	−2·027
0·45	0·101	0·021	0·2460	2·013	0·080	−2·013	−0·031	−0·2459	−0·2459	−2·013
0·40	0·202	0·072	0·2459	2·023	0·127	−2·023	−0·120	−0·2459	−0·2459	−2·024
0·35	0·304	0·140	0·2459	2·058	0·142	−2·058	−0·237	−0·2459	−0·2459	−2·058
0·30	0·408	0·207	0·2459	2·090	0·127	−2·091	−0·353	−0·2459	−0·2459	−2·091
0·25	0·512	0·260	0·2459	2·075	0·085	−2·075	−0·442	−0·2459	−0·2459	−2·076
0·20	0·613	0·288	0·2459	1·959	0·025	−1·959	−0·484	−0·2459	−0·2459	−1·960
0·15	0·704	0·283	0·2459	1·703	−0·043	−1·704	−0·471	−0·2459	−0·2459	−1·704
0·10	0·779	0·245	0·2459	1·298	−0·107	−1·298	−0·405	−0·2459	−0·2459	−1·298
0·05	0·831	0·180	0·2459	0·761	−0·156	−0·761	−0·295	−0·2459	−0·2459	−0·762
0·00	0·853	0·095	0·2459	0·141	−0·182	−0·141	−0·155	−0·2459	−0·2459	−0·141
−0·05	0·844	0·003	0·2459	−0·500	−0·182	0·501	−0·002	−0·2459	−0·2459	0·501
−0·10	0·804	−0·081	0·2459	−1·096	−0·156	1·096	0·149	−0·2459	−0·2459	1·097
−0·15	0·737	−0·147	0·2459	−1·588	−0·108	1·589	0·280	−0·2459	−0·2459	1·589
−0·20	0·649	−0·185	0·2459	−1·939	−0·045	1·939	0·372	−0·2459	−0·2459	1·939
−0·25	0·547	−0·191	0·2459	−2·139	0·021	2·139	0·409	−0·2459	−0·2459	2·140
−0·30	0·438	−0·166	0·2459	−2·213	0·077	2·213	0·381	−0·2459	−0·2459	2·214
−0·35	0·328	−0·119	0·2459	−2·210	0·109	2·210	0·291	−0·2459	−0·2459	2·211
−0·40	0·218	−0·065	0·2459	−2·184	0·109	2·184	0·164	−0·2459	−0·2459	2·185
−0·45	0·109	−0·019	0·2459	−2·174	0·074	2·174	0·046	−0·2459	−0·2459	2·174
−0·50	0·000	0·000	0·2459	−2·185	0·003	2·185	−0·009	−0·2459	−0·2459	2·185

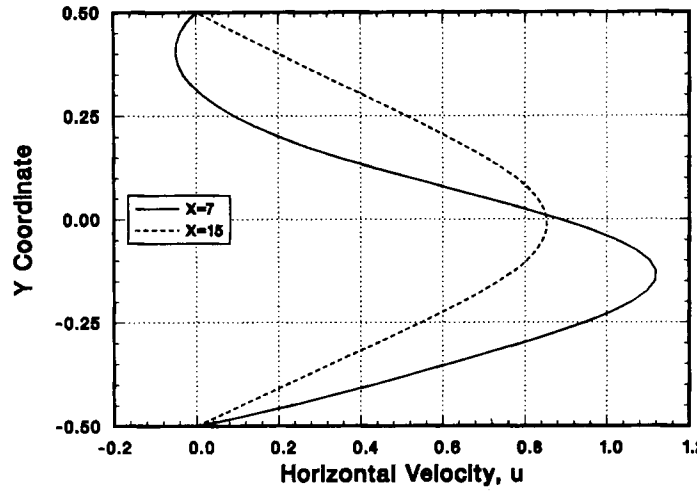

Figure 9. Horizontal velocity profiles across the channel at $x=7$ and 15, Backward Facing Step–$Re=800$

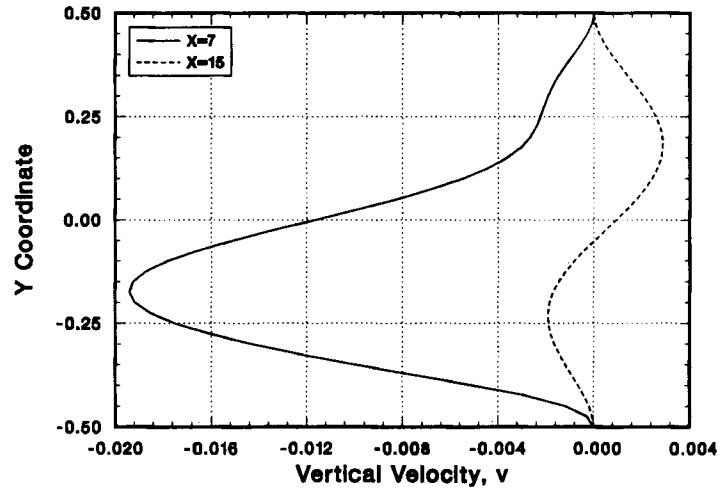

Figure 10. Vertical velocity profiles across the channel at $x=7$ and 15, Backward Facing Step–$Re=800$

5.2. *Cross-channel profiles*

In order to provide data for the evaluation and/or development of various outflow boundary conditions, cross-channel profiles of a variety of quantities are provided in Tables IV and V; some of these data are also illustrated in Figures 9–14. The profiles are located at 14 ($x=7$) and 30 ($x=15$) step heights downstream of the step. It is evident from the tabulated data and the plots that there is considerable cross-channel variation in many quantities, making their utility as a potential boundary condition questionable. The streamwise gradients of velocity (Figure 13) are generally 'small' but are not really zero as often assumed in some boundary specifications. The

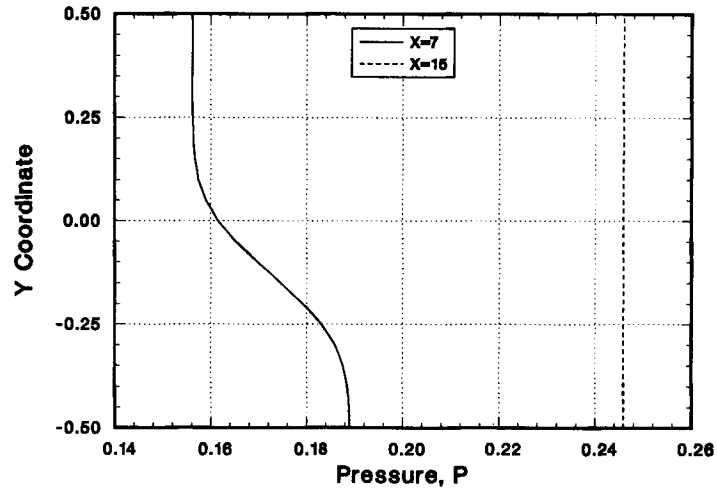

Figure 11. Pressure profiles across the channel at $x=7$ and 15, Backward Facing Step–$Re=800$

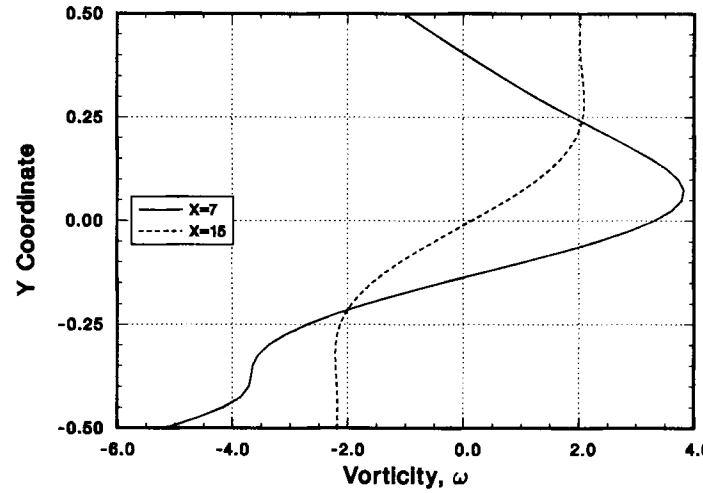

Figure 12. Vorticity profiles across the channel at $x=7$ and 15, Backward Facing Step–$Re=800$

total normal stress quantities involving the pressure and streamwise velocity gradient (Figure 14) show an almost constant value, especially at the $x=15$ location. The normal stress is essentially equal to the pressure since both μ and $\partial u/\partial x$ are small. A constant normal stress condition is typically used in finite element methods for outflow boundaries and these results show why that choice can be effective.

The variation of some of the variables in the vicinity of the step is also of interest owing to their singular behaviour at this location. Shown in Figures 15 and 16 are cross-channel profiles of the pressure and vorticity taken at the inlet plane, $x=0$. Results for two different mesh refinements

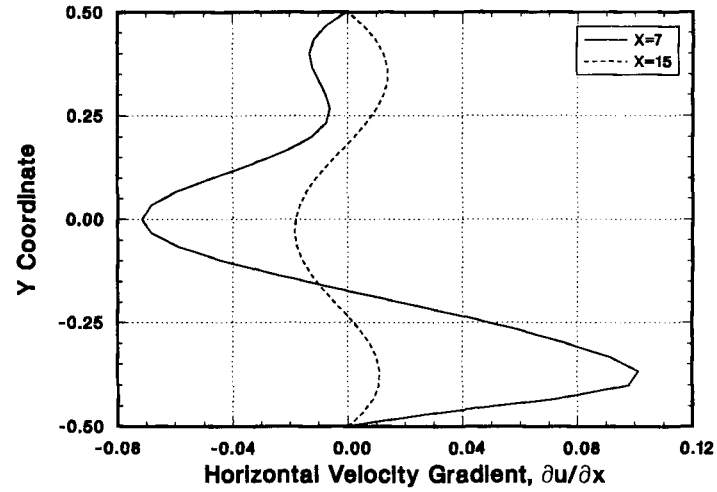

Figure 13. Horizontal velocity gradient across the channel at $x=7$ and 15, Backward Facing Step–$Re=800$

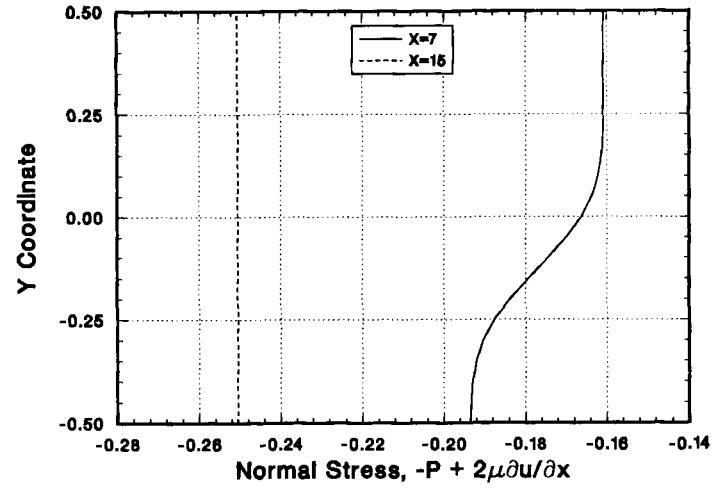

Figure 14. Total normal stress across the channel at $x=7$ and 15, Backward Facing Step–$Re=800$

are shown and it is clear that the resolution of the sharp gradients (slopes) at the corner is less than satisfactory. At $y=0$ the slope of each curve varies directly with the mesh spacing, which is suggestive of a singular behaviour. However, at relatively small distances from the corner the solutions are well behaved and the vorticity becomes identical for the two mesh refinements. Note that the large apparent discrepancy in the pressure is exaggerated by the scale of the plot. The pressure levels between the two simulations differ by 0·005 (with a pressure maximum in the field of $P_{max}=0{\cdot}251$), which is less than 2%. This result also emphasizes the fact that the pressure is a very sensitive variable in an incompressible flow.

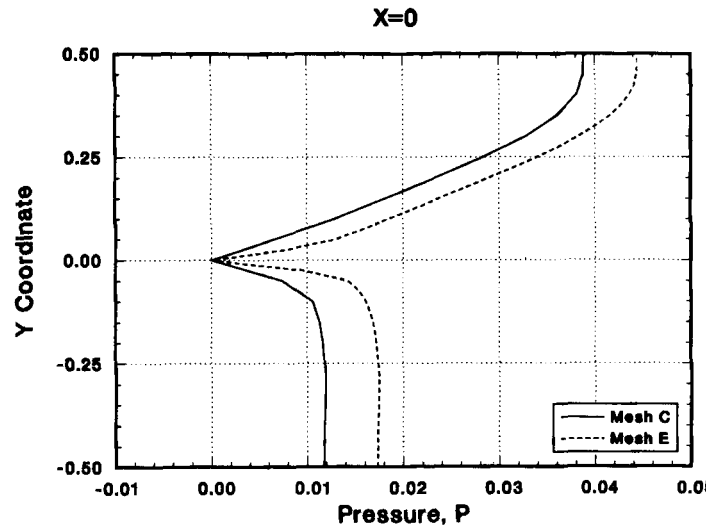

Figure 15. Pressure profiles across the channel at the inlet plane for two mesh refinements, Backward Facing Step–$Re = 800$

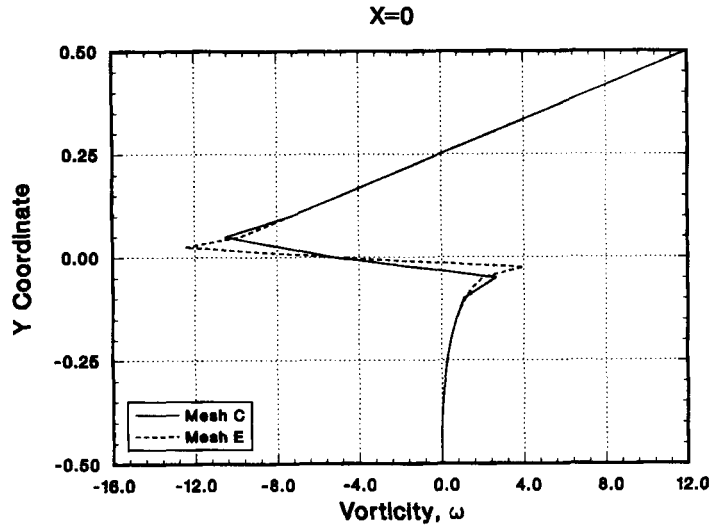

Figure 16. Vorticity profiles across the channel at the inlet plane for two mesh refinements, Backward Facing Step–$Re = 800$

6. CONCLUSIONS

The work reported here is an attempt to provide a fully converged and accurate solution to a standard test problem. The backward-facing step flow was selected as a test problem since it is one of the simplest geometric cases that provides an interesting, non-trivial flow that is a good test for outflow boundary conditions. The separation zones downstream of the step provide a sensitive measure of the quality of the outflow condition and how its location along the channel

influences the solution. Sufficient data have been reported to allow outflow boundary conditions to be tested and compared to this benchmark. Even without the development of new boundary conditions it is instructive to examine the variation of a variety of variables across the channel and assess their potential as boundary conditions.

ACKNOWLEDGEMENTS

This work was performed at Sandia National Laboratories and supported by the U.S. Department of Energy under Contract Number DE-AC04-76DP00789.

REFERENCES

1. B. F. Armaly, F. Durst, J. C. F. Pereira and B. Schonung, 'Experimental and theoretical investigation of backward-facing step flow', *J. Fluid Mech.*, **172**, 473–496 (1983).
2. D. K. Gartling, 'NACHOS II—a finite element computer program for incompressible flow problems', *SAND86-1816* and *SAND86-1817*, Sandia National Laboratories, Albuquerque, NM, 1987.
3. *FIDAP Theoretical Manual, Version 4.5*, Fluid Dynamics International, Evanston, IL, 1988.
4. D. K. Gartling, 'MERLIN II—a computer program to transfer solution data between finite element meshes', *SAND89-2989*, Sandia National Laboratories, Albuquerque, NM, 1990.
5. J. Kim and P. Moin, 'Application of a fractional-step method to incompressible Navier–Stokes equations'. *J. Comput. Physics*, **59**, 308–323 (1985).
6. J. Sohn, 'Evaluation of FIDAP on some classical laminar and turbulent benchmarks'. *Int. j. numer. methods fluids*, **8**, 1469–1490 (1988).